LDV Measurement of Swirl Flow in Internal Combustion Engines

J. Katoh, Y. Ohkubo, M. Ohtsuka and K. Sugiyama
TOYOTA Central Research and Development Laboratories, Inc.
Nagakute-cho, Aichi-gun, Aichi-ken, 480-11

ABSTRACT

The purpose of this study is to investigate the relation between the in-cylinder swirl characteristics and the steady-state swirl ratio of intake port. The swirl velocity distributions in a cylinder radius were measured by LDV for two combustion chamber shapes; flat piston and cylindrical bowl piston. In either case, the swirl ratio was systematically changed by employing several different port geometries.

In the case of flat piston, the swirl velocity profiles during compression and early expansion stroke have a similar to solid body rotation configurations irrespective of the swirl ratio. In the case of cylindrical bowl piston, the velocity distributions near TDC are different for different swirl ratios. At higher ratios, the profile remains linear, but, at lower ratios, it becomes non-linear.

INTRODUCTION

A knowledge of the flow phenomena inside the cylinder is necessary for optimum design of the intake port and the piston cavity configurations. Recent trends toward smaller direct-injection diesel engines have increased the need for clear understanding of the flow field, especially the swirl characteristics. The swirl flow is an essential parameter to affect the air-fuel mixing, combustion efficiency, therefore the engine performances.

Traditionally, the swirl generating capability of intake port is estimated by a test under steady-state. In the test, the swirl angular velocity or momentum is measured by a vane type flow meter (1) or an impulse meter (2). Then, the swirl ratio is determined under an assumption of the quasi-steady state during intake stroke. However, the ratio does not exactly represent the swirl characteristics under operating condition because the air motion in the test is different from that of operating engine. And the ratio provides no information about the change of swirl during compreesion. Accordingly, the swirl flow field near TDC must be observed by means of direct measurement for in-cylinder gas velocity.

In recent years, Laser Doppler Velocimetry has been developed and applied to measurement of the flow velocity of gases in the internal combustion engines (3). And numerous results have been revealed on various aspects of the swirl flow (4-15). However, it is difficult to say that the whole phenomena of swirl flow have been completely cleared, such as the effect of port and chamber geometries on the swirl characteristics (15). Another problem is that most previous works have used model engines which were modified from actual engine geometry for optical access. A few studies used the actual engine geometry for velocity measurement (10-13). Accordingly, the experimental results from those model engines are not suitable to interpret the actual engine characteristics or performances.

The purpose of this study is to investigate the relation between the characteristics of in-cylinder swirl flow field and the steady-state swirl ratio of intake port. For this purpose, we used a research engine, developed by TOYOTA Central Research and Development Laboratories and called the "bottom-view engine", which has a cylinder head whose intake port configuration and valve locations are almost the same as actual engines. Therefore, the air motion inside the cylinder is similar to the real one. The swirl velocity profile was measured by a backscatter LDV for two combustion chamber shapes; flat piston and cylindrical bowl piston. In eihter case, the swirl ratio of intake port was systematically changed by using several different port configurations.

EXPERIMENTAL APPARATUS AND PROCEDURE

Test Engine

A single-cylinder research engine was developed to measure the velocity component in the combustion chamber by LDV. Its specifications are shown in Table 1.

For optical access, the engine has a hollow long piston with a quartz window at the piston crown, as schematically shown in Figure 1 (the bowl piston case is shown). Through the window, the state inside the cylinder is visualized from the bottom side. So, the engine is called the "bottom-view engine". The combination of this engine and a backscatter LDV allows the velocity measurement inside the cylinder.

The piston crown attachment is replaceable to compose various types of combustion chambers. In this study, two chamber configurations are used; (1) flat piston and (2) centrally located

Table 1 Engine specifications

Type	4-stroke	OHV
Bore	83 mm	
Stroke	85 mm	
Swept volume	460 cm^3	
Top clearance	8.8 mm	(flat piston)
	0.6 mm	(bowl piston)
Compression ratio	10.0	(flat piston)
	17.8	(bowl piston)
Valve timing		
Intake open	TDC	
close	35 degrees	ATDC
Exhaust open	58 degrees	BBDC
close	TDC	

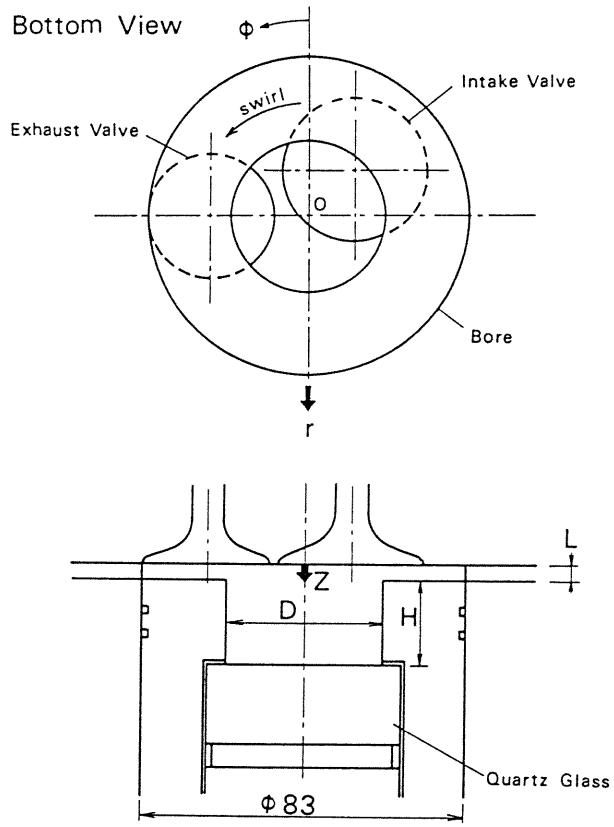

Combustion chamber	D	H	L (mm)
Flat piston	- -	- -	8.8
Bowl piston	33.6	22.6	0.6

Fig.1 Combustion chamber geometry

cylindrical bowl piston. These dimensions are also shown in Figure 1.

In the case of flat piston, the top clearance and compression ratio are set to be 8.8 mm and 10.0, respectively. A quartz glass, flush with the piston surface, is available for visualizing the space within the radius of 30 mm from the cylinder axis. In the case of bowl piston, the top clearance and compression ratio are set to be 0.6 mm and 17.8, respectively. This is more realistic condition than that of

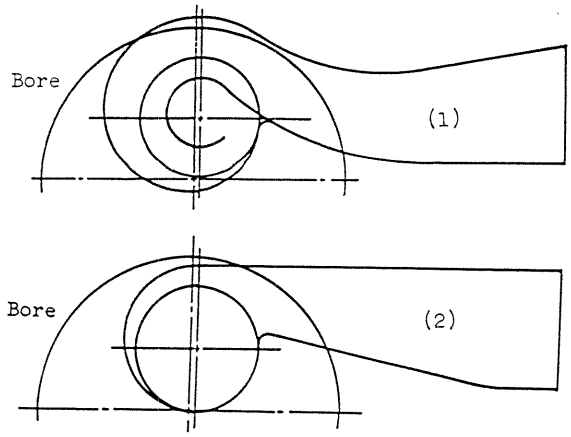

Fig.2 Typical port shapes for two chamber case
(1) flat piston case
(2) bowl piston case

Table 2 Series of steady-state swirl ratios for two chamber cases

Case	Swirl Ratio			
Flat piston	4.3	3.4	2.6	
Bowl piston	3.6	3.0	2.6	1.1

flat piston. The whole region within the bowl is visible since a quartz glass is located at the bottom of the bowl (see Fig. 1).

As the window is located at the piston, the cylinder head is not necessary to be modified for optical access. Therefore, the head geometry, such as intake port configuration and intake exhaust valve locations, are constructed in the same constitution as in actual engines. So, the air motion generated by the port is similar to that in the actual engines because the induced swirl flow during intake stroke depends upon the port configuration.

As the cylinder head is exchangeable, the either of several heads that have different port shapes each other is installed in order to change the swirl ratio. These port configurations are basically grouped in two types for two chamber cases. Figure 2 shows the two typical geometries; (1) flat piston case and (2) bowl piston case. The ratios are systematically changed in order to investigate the relation between the swirl ratio and the in-cylinder swirl velocity, as shown in Table 2.

The swirl flow has the counterclockwise direction in all cases when the head is seen from the bottom side of the engine, as shown in Figure 1.

The swirl ratio, which is defined as the ratio of the solid body rotation angular velocity to the engine speed, is determined by the vane type swirl rig test in a steady-state (1). And the ratio is expressed by the equation (1), as follows.

$$SR = \frac{1}{Ne} \cdot \frac{\int Ga \cdot Ns \, dt}{\int Ga \cdot dt} \qquad (1)$$

where Ga is mass flow rate of intake air, Ne is engine revolution, Ns is swirl angular velocity determined by the rotational frequency of the vane. The integration ranges from TDC to BDC in the intake stroke.

Laser Doppler Velocimeter System

The dual-beam, backscatter LDV system is used. The specifications are shown in Table 3 and the constructions are shown in Figure 3 schematically.

The optical access is accomplished as follows.

A laser beam from the laser tube is divided into two beams in a horizontal plane by a beam-splitter. Then, the beams are led to the beam-expander so as to expand their diameter and to the lens system for focusing. In the optical system, one of the beams is shifted in its frequency by a Bragg-Cell to determine the flow direction. The two beams from the focusing lens are reflected by a mirror located at the cylinder block and led into the combustion chamber from the bottom side of the engine through the quartz window at the piston, then cross at a measurement location. The scattered light from the measurement volume go backward and are collected by the focusing lens and detected by a photomultiplier.

The doppler signals are processed as follows.

To begin with, the signals are electrically mixed by a mixer to a selected frequency level since the Bragg-Cell has raised signal frequency by 40 MHz. Next, the mixed signals are processed by a frequency counter. At the counter the doppler signals are filtered out to remove higher and lower frequency noises. Then the filtered signals are converted to the voltage which is the inversely proportional of the signal frequency. To select a reasonable band-pass filter range is very important for noise reduction. However, it must be usually selected by trial-and-error for individual measurements.

The measurement locations are set up by traversing the optical system.

Table 3 LDV specifications

Laser wavelength	514.5 nm
Laser power	250 mW (used. 1.2 W max.)
Focal length of focusing lens	750 mm
Beam crossing angle	10.01°
Measurement volume	
Waist diameter	0.2 mm
Length	2.6 mm
Fringe spacing	2.95 μm

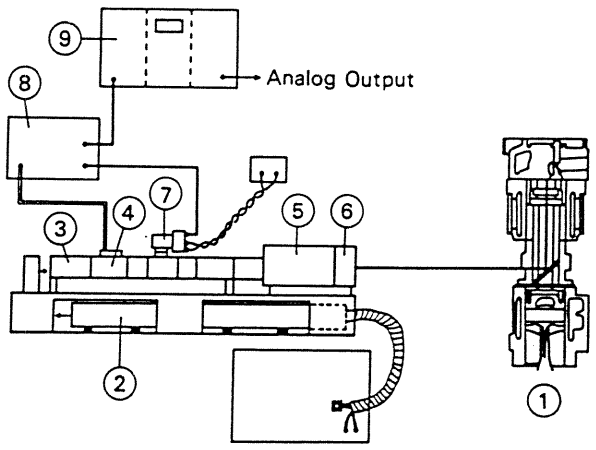

Fig.3 Schematic illastration of LDV system
(1) "bottom-view" engine (2) Ar-ion laser
(3) beam-splitter (4) Bragg-Cell
(5) Beam-expander (6) Focusing lens
(7) Photomultiplier (8) Frequency mixer
(9) Frequency counter

Seeding. A seed generating device, in which seeding particles and by-pass air from surge tank were mixed, supplied the seeding air into the intake manifold. As the by-pass air was pressed by a blower, the amount of air flow was increased during intake. But the increase of volumetric flow rate was less than 5 % and was negligible.

Titanium Dioxide (TiO_2, mean diameter 0.3 μm) was used as the seeding material.

Data Aquisition and Processing

Analog outputs after frequency-voltage conversion in the counter are digitized by an A/D converter and aquired by a mini-computer system (VAX11/730/750). For obtaining the time-dependent data, the real-time sampling for each crank-angle is carried out.

The aquired data are first stored in the computer disk memory. After the measurement, the data are moved to a magnetic tape for off-line data processing. In off-line processing, the digitized voltage data are restored to the disk memory from the magnetic tape. Then, they are converted to the values of instantaneous velocities corresponding to individual crank-angles. After that, an ensemble-averaged mean velocity for each crank-angle is calculated from those instantaneous velocity data.

The mean velocity profile has practical importance in the case of direct-injection diesel engine because the structure of velocity field essentially affects the air-fuel mixing before combustion on the whole. To obtain an accurate ensemble-averaged value, the data are aquired about more than 400 cycles of engine operation in a single measurement. In general, the backscatterd light is not so intense as the forwardscattered. As the result, it is difficult to obtain such a large number of data in each cycle to enable the cycle-to-cycle resolution. Actually, the data rate is not so sufficient to obtain the cycle-resolved velocity data in this measurement. So, the cyclic variation is not considered in this study.

Experimental Condition

All the measurements were made under motored condition at an engine speed of 600 or 900 rpm.

The throttle was wide-opened.

Lubricating oil was not fed to the piston during each measurement to keep the optical window clear.

Measurement location and coordinate system. A cylindrical polar coordinate (r,Φ,z) system is used to describe the locations of the measurement points, as shown in Figure 1. The cylinder axis is defined as the z-axis with the cylinder head surface as $z = 0$. The radial distance from the cylinder axis is defined as r. The angle from

the engine front is defined as Φ whose direction is counterclockwise as seen from the bottom side the cylinder.

LDV measurements were made in the same direction of Φ = 180, which corresponds the direction from the chamber center toward the engine rear direction, in all cases. In the case of flat piston, measurements were made at 6 locations every 5 mm from r = 0 to r = 25 at z = 4.4 plane which corresponds to the midplane in the clearlance volume. In the case of bowl piston, measurements were made at 9 points every 2 mm from r = 0 to r = 16 at z = 12 in the near-mid plane of the combustion bowl at TDC. Figure 4 shows the measurement locations in each case.

The swirl velocity is defined as the velocity component of Φ. And positive sign is defined as counterclockwise direction as seen from the bottom view in Figure 1, which corresponds to the induced swirl flow direction.

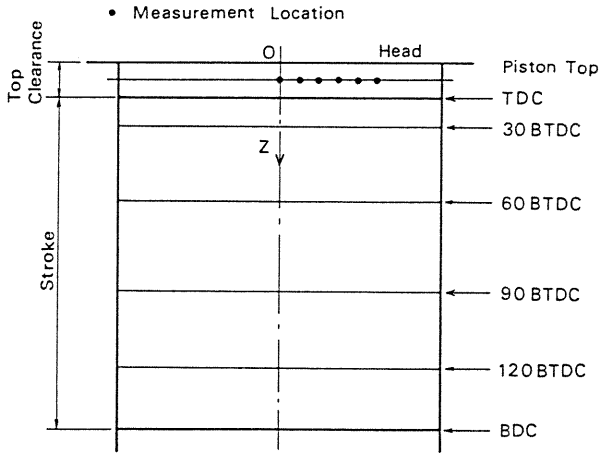

(1) flat piston case

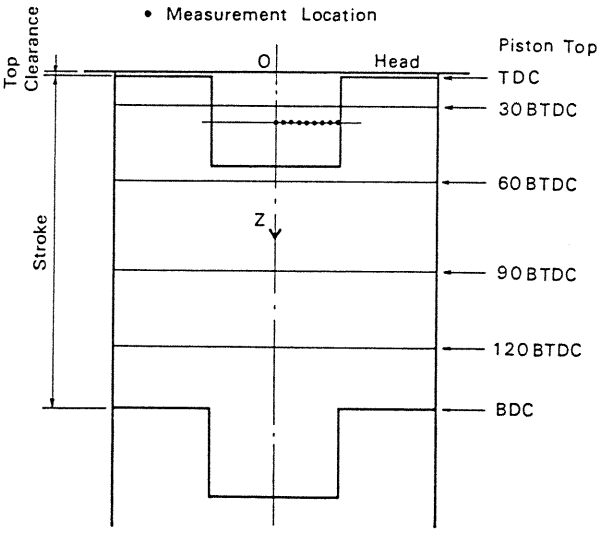

(2) bowl piston case

Fig.4 Measurement locations

RESULT AND DISCUSSION

Flat Piston Case

Summaries of the data for flat piston case are presented on Figures 5 and 6, for an engine speed of 600 rpm.

Figure 5 shows the swirl velocity distributions along the measurement locations and their change during compression and early expansion stroke after the intake-valve closed. The parallelogram lines in each figure show the zero-velocity plane. The lines going up toward the right indicate the radial distance and the lines going up toward the left indicate the crank-angle. The height from the zero-velocity plane at a radial distance and a crank-angle indicates the velocity magnitude. The reference height beside each figure shows 10 m/s.

Figire 6 also shows the same data represented by the contour mapping. In each figure, the axis of abscissas and the axis of ordinates indicate the radial distance and the crank-angle, respectively. The contour lines are drawn at an interval of 1 m/s and the additional numerical values show the velocity for the line. The slashed parts show the maximum velocity region of each data.

Two main characteristics are seen from all these figures. First, the velocity increase along radial distance and the profiles nearly show solid body rotation during compression and early expansion stroke. Second, it is seen that the velocity makes a wavy variation against crank-angle.

These characteristics are the same for different swirl ratios. So, it is considered that the flow field in this case is similarly wavy for any swirl ratio.

To understand the detail, the profiles near TDC are given in Figure 7. The swirl velocity increases almost linearly with the radial distance irrespective of the swirl ratio, though the slope of profile depends upon the swirl ratio and varies against crank-angle. These results are in agreement with those of previous works at the point that the swirl is solid body rotation type (5,6,8). So, in this case, the solid body rotation pattern is essential for swirl flow.

Figure 7 also shows the profile at early compression stroke (120 degrees BTDC) that indicates the initial swirl after the valve closed. In the figure, the slope of distribution does not clearly show to be dependent on the swirl ratio, though the patterns also show a linearity. The profile may not be representative of initial swirl flow since the data has been obtained near the head plane alone (see Fig. 4). It is believed that the swirl profiles are not homogeneous along the cylinder axis.

The variation of swirl velocity versus crank-angle for three different swirl ratios are shown in Figure 8, at the points of r = 25 and r = 5. From the figure, it is seen that the velocity takes a minimum and a maximum value during compression stroke. The minimum points are taken at 50-70 degrees BTDC, the maximum points are taken at 10-40 degrees BTDC, which are different for different swirl ratios. In either ratio, the crank-angles at the minimum and maximum points correspond with those of all measured locations. But the amplitude of the variation becomes larger toward the cylinder axis, and it increases as the swirl ratio increases, as also seen in the figure.

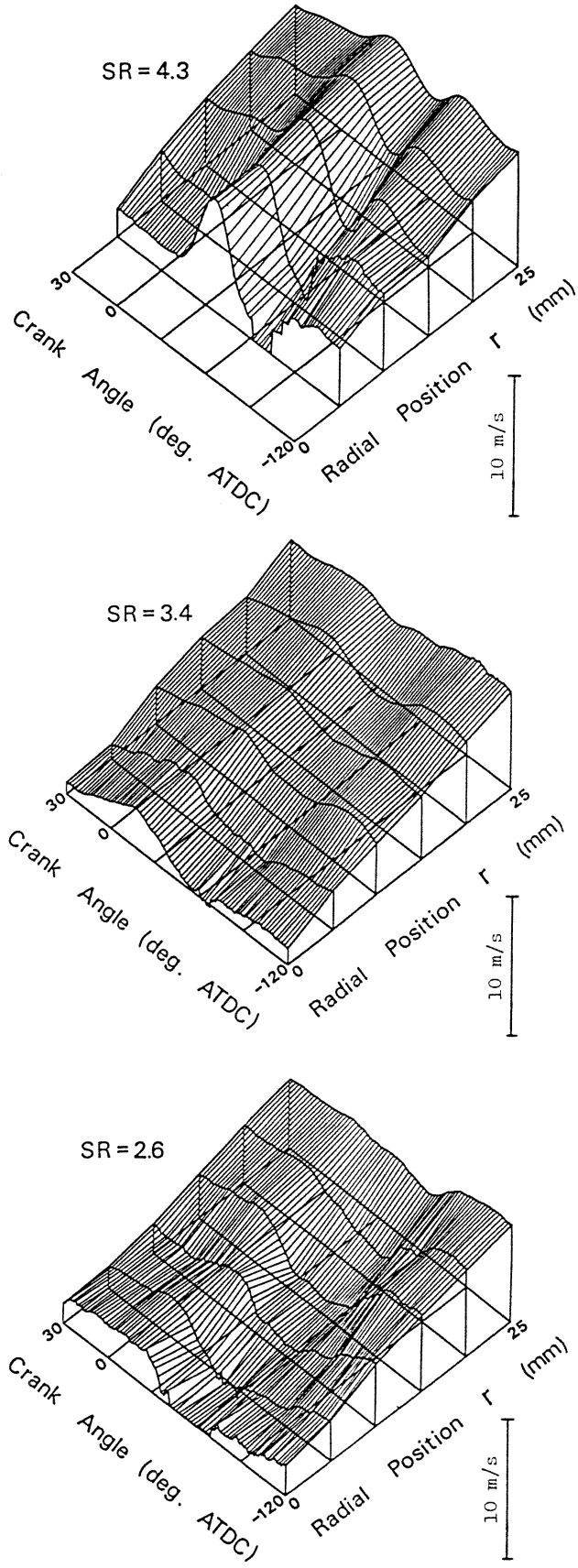

Fig.5 Stereographic projections of measured data for different swirl ratios (flat piston, 600 rpm)

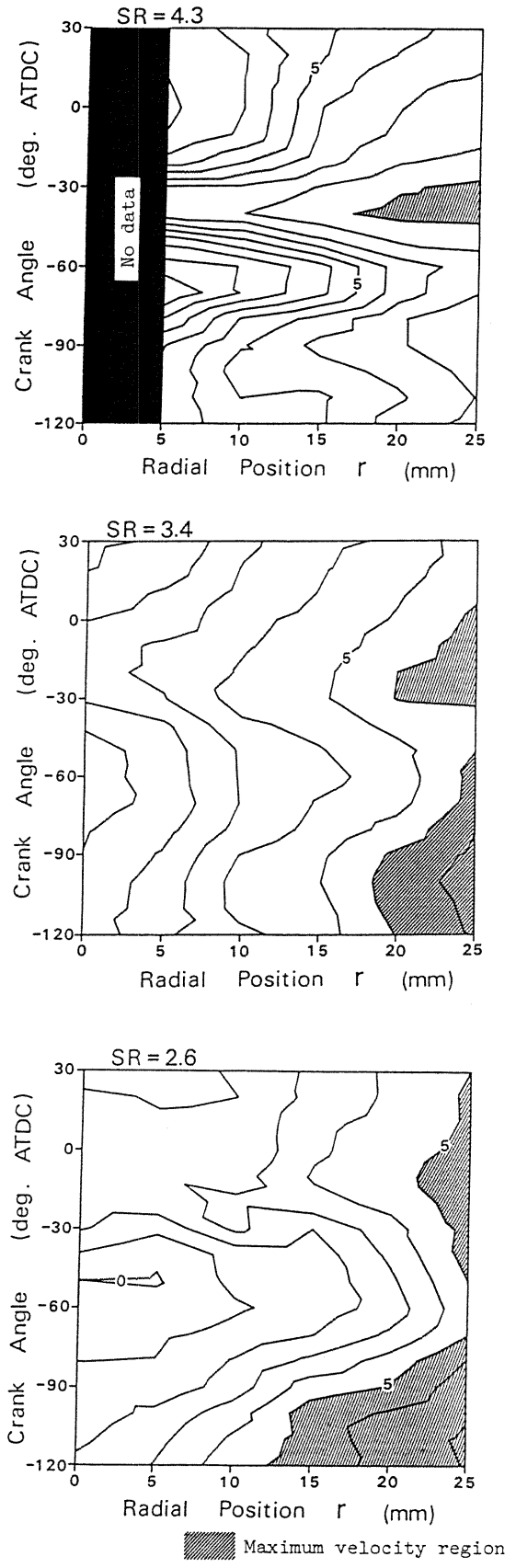

Fig.6 Contour maps of swirl velocity distribution (flat piston, 600 rpm)

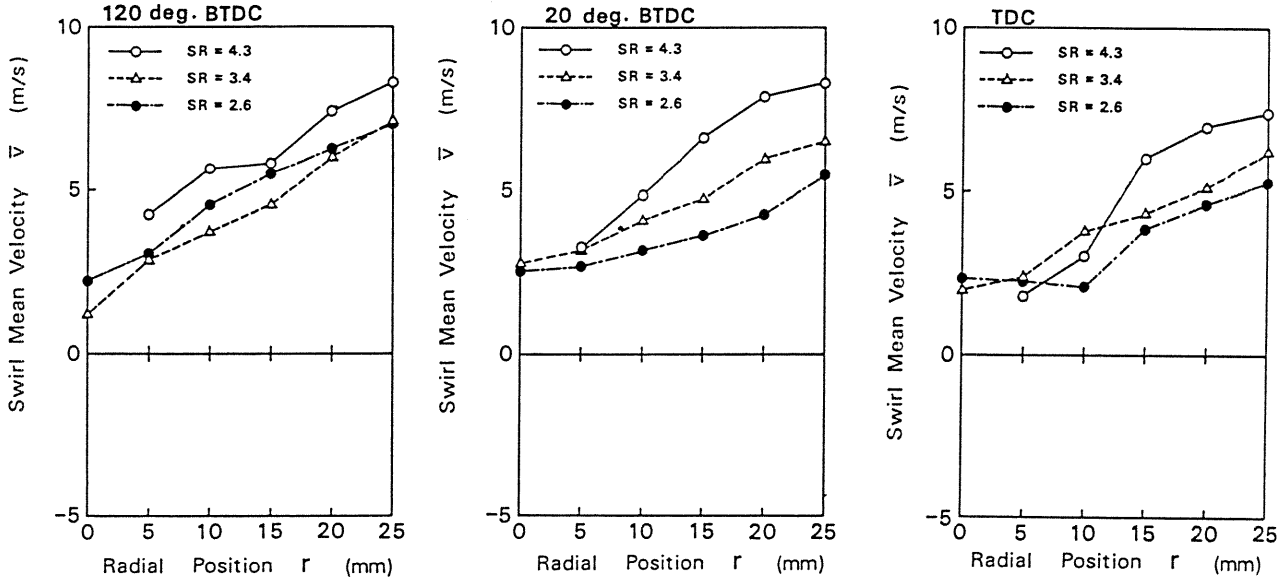

Fig.7 Swirl velocity profiles for different swirl ratios at TDC, 20 deg. BDTC, and 120 deg. BTDC (flat pison, 600 rpm)

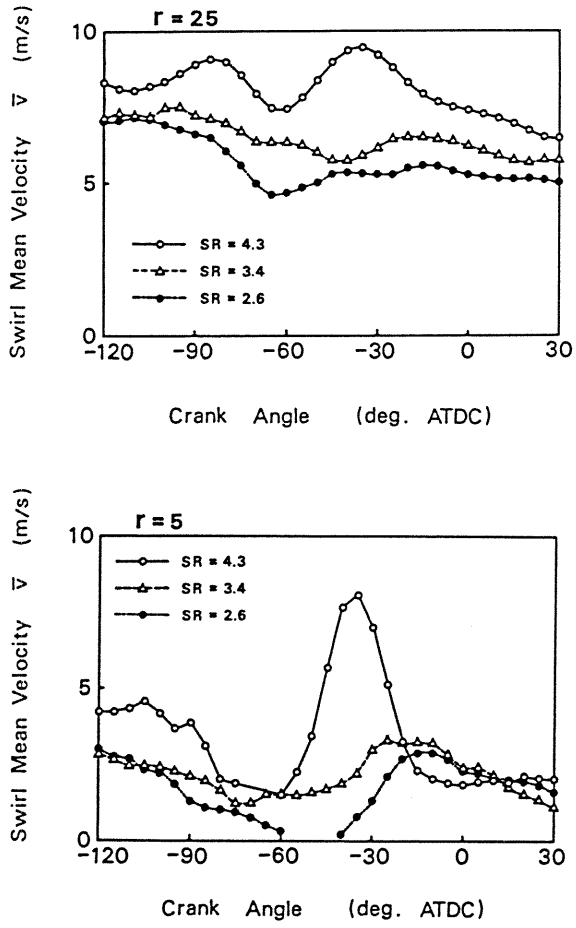

Fig.8 Velocity variations versus crank-angle for different swirl ratios at r = 25 and r = 5 (flat piston, 600 rpm)

These results suggest that the flow field is not simple but has strong 3-dimensionality even in this flat piston case as Rask pointed out (5). Actually, in Figure 7 the velocity at the cylinder axis is not zero which means that the swirl flow is not axis-symmetric. And even in the recent progressive theoretical study such as the multi-dimensional model simulation, the solution with an assumption of axis-symmetry gives monotonous decay with the swirl velocity during compression (16).

Cylindrical Bowl Piston Case

Summaries of the data for cylindrical bowl piston case are presented in Figures 9 and 10, for an engine speed of 600 rpm. These figures are represented in the same form as in Figures 5 and 6. It should be noted that the radial distance is different from that in Figures 5 and 6.

From these figures, it is seen that the flow phenomena show considerable difference from those in the case of flat piston. The ways in which the swirl velocity distribution varies during compression and early expansion stroke are not similar for different swirl ratios. The characteristics of flow phenomena are roughly divided into two types according to the swirl ratios. At higher ratios (3.6, 3.0), the velocity toward the bowl periphery rapidly increases during compression stroke. On the other hand, at lower ratios (2.6, 1.1), the increasing rates of swirl velocity are not the same along the radial direction. The velocity increase is remarkably reduced toward the bowl periphery. It is clearly seen in Figure 10 that the maximum velocity region moves from the bowl periphery toward the cylinder axis, as the swirl ratio decreases.

To explore the detail, the typical profiles at early and late compression are given in Figure 11. The swirl velocity profiles always show different shapes for different swirl ratios. For the swirl ratio of 3.6, the distribution during compression almost indicates a solid body rota-

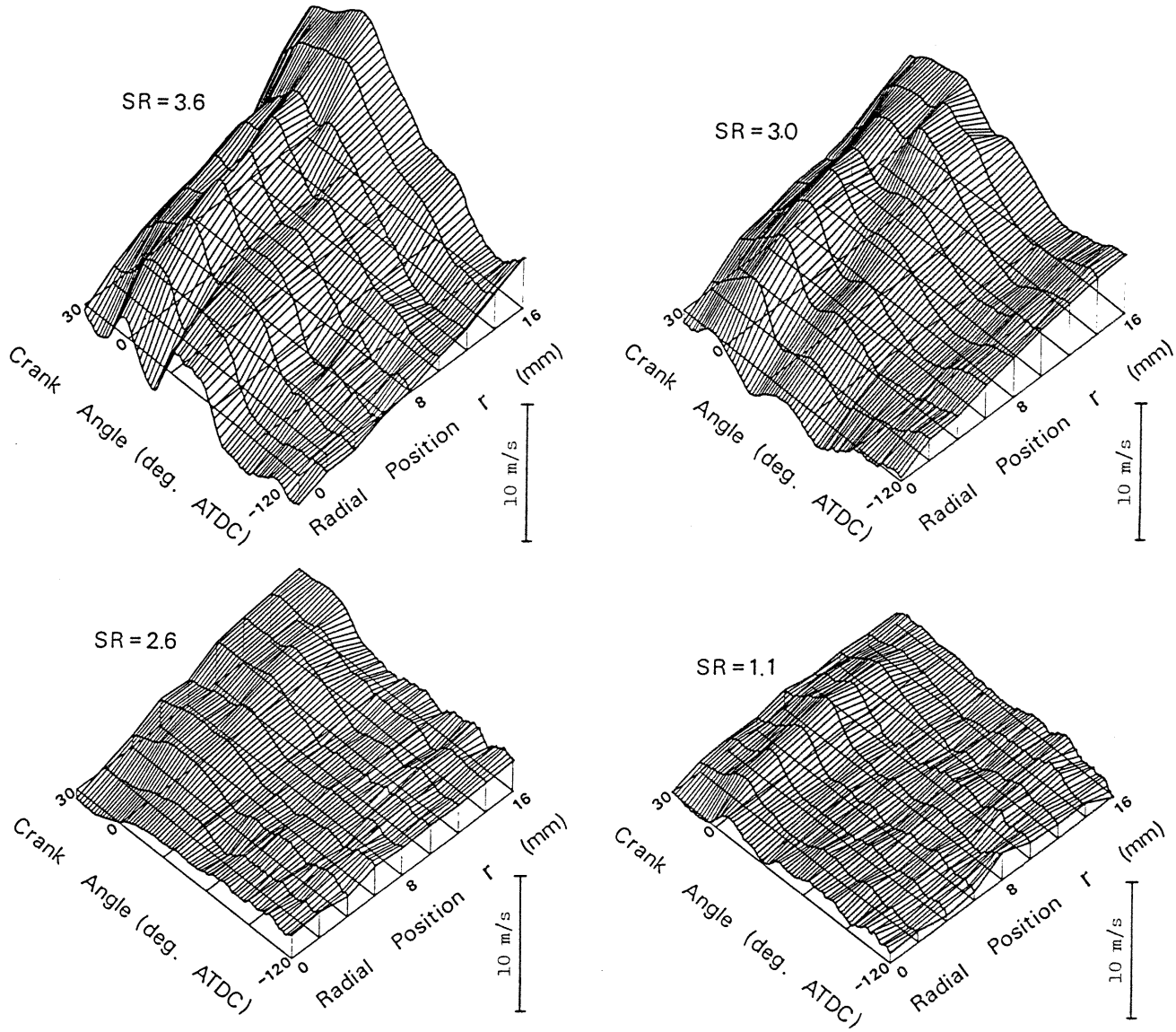

Fig.9 Stereographic projections of measured data for different swirl ratios (bowl piston,600 rpm)

tion pattern that is similar to the case of flat piston although the increase of the slope near TDC noticeably larger than that of flat piston. For the ratio of 3.0, the pattern near TDC resembles to that of 3.6 in character. But the profile departs from linearity near the bowl periphery at 20 degrees BTDC, and slightly tapers off toward the periphery at TDC. As the swirl ratio decreases, the profile takes a manifest non-linear pattern near TDC. It is certainly shown that the velocity decreases from about half the radius toward the bowl periphery at TDC for the ratio of 1.1.

In this case, strong squish flow may exert much influence on the swirl flow to form a complicated flow pattern (14). At higher ratios, it acts to compress the swirl into the combustion bowl and to make an appreciable velocity increase near TDC. At lower ratios, it behaves as a barrier to prevent the swirl from progressing toward the bowl rim.

At 120 degrees BTDC, the profiles are also dissimilar for different swirl ratios. And at lower ratios, they differ from a solid body rotation type. It suggests that an obvious swirl is not formed initially at lower ratios. However, it should be noted that the results are not representative of initial swirl throughout the cylinder since the profiles have been obtained in the comparatively small region of near the head and the cylinder axis (see Fig. 4).

The variation of swirl velocity versus crank-angle for four different swirl ratio are shown in Figure 12, at the points of r = 16 and r = 4. The changing manner is also different for different swirl ratios though the velocity depends upon the swirl ratio.

Near the bowl periphery (r = 16), the two higher ratio cases, SR = 3.6 and SR = 3.0, show the remarkable velocity increase during compression, and take a peak around 10 degrees BTDC. In these cases, the velocity increase begins about 90 degrees BTDC which corresponds to the half stroke of compression. Therefore, the

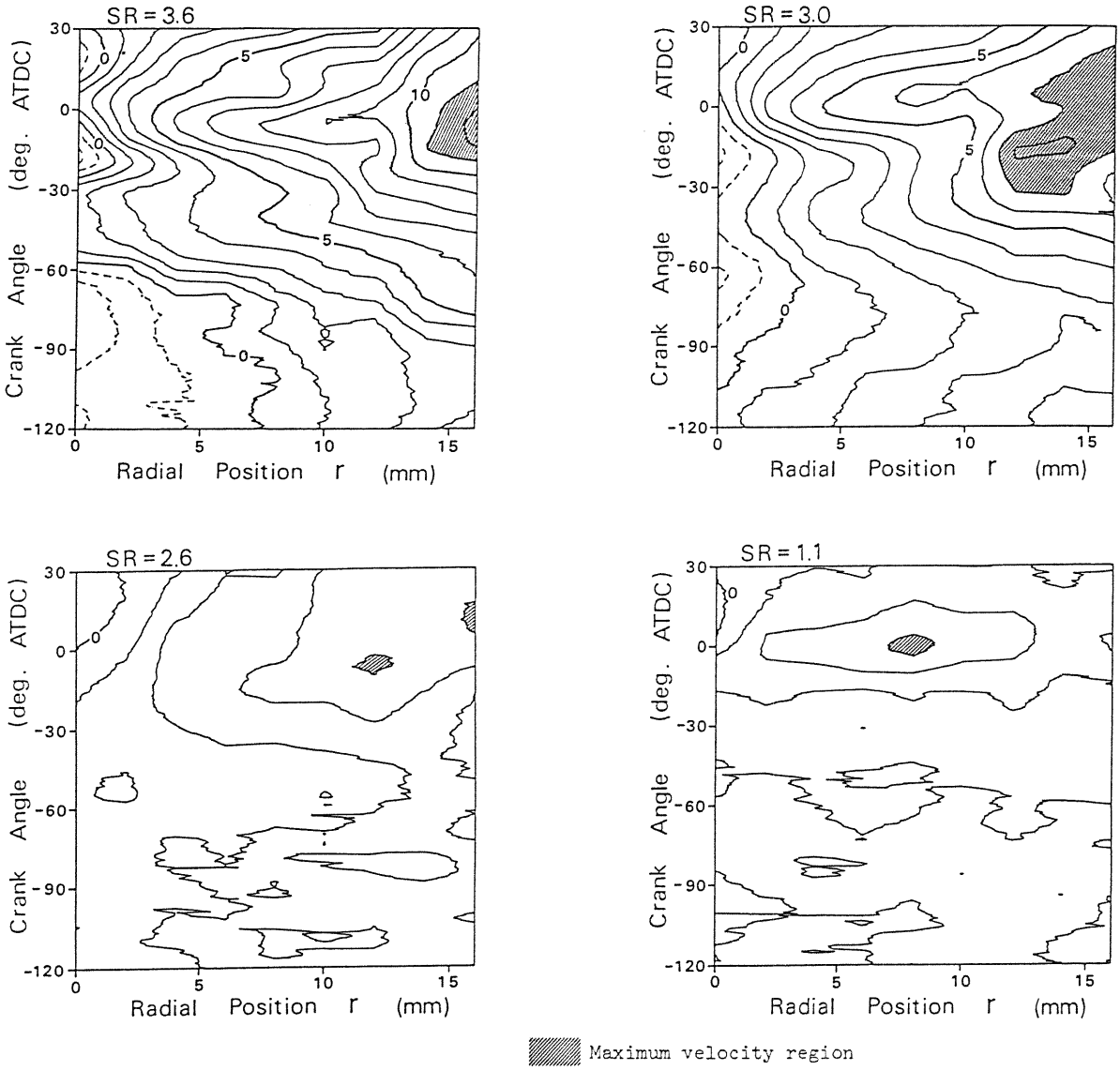

Fig.10 Contour maps of swirl velocity distribution (bowl piston, 600 rpm)

effect of chamber shape appears after at least half the stroke of compression. Contrarily, the lower ratio cases show the small variation of the velocity. For the ratio of 2.6, the velocity increase appears only near TDC. For the ratio of 1.1, the velocity remains approximately constant in a low quantity. Therefore, at lower ratios, the swirl scarecely exists near the bowl periphery.

Near the cylinder axis (r = 4), the velocity keeps a low value for either swirl ratio throughout the compression stroke. However, the variating patterns are still in this case separated into two types for higher swirl ratios and lower ratios. At higher ratios, the velocity increase begins about 60 degrees BTDC and takes two peaks in late compression. The first peak appears at a time when the piston top has crossed the measurement plane, and the second peak occurs just before TDC. At lower ratios, the velocity increase appears at late 30 degrees BTDC.

These results clearly indicate that the difference of swirl ratio influences not only the spacial swirl distribution but also the time-dependent manner of swirl velocity.

In Figure 12, the negative velocity is indicated at 60-120 degrees BTDC of SR = 3.6 at r = 4. It suggests that the swirl has an off-axis center of rotation. Actually, the swirl profile does not show axis-symmetric, as also seen in Figure 11. In this case, the deformation from axis-symmetric seems to be less than that of flat piston.

Swirl Ratio

The equivalent swirl ratio that represents the swirl intensity has been calculated from the measured velocity distribution at TDC. The equivalent ratio is determined from the slope of an equivalent solid body rotation profile with the same angular momentum as that of the measured velocity distribution. It is obtained from the

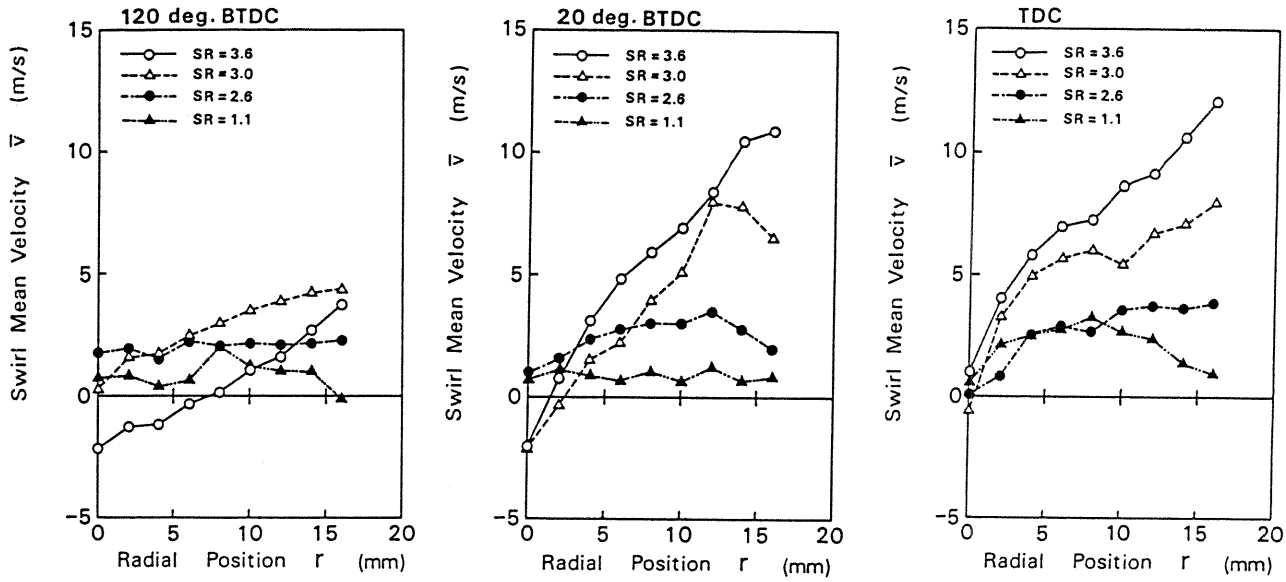

Fig.11 Swirl velocity profiles for different swirl ratios at TDC, 20 deg. BTDC, and 120 deg. BTDC (bowl piston, 600 rpm)

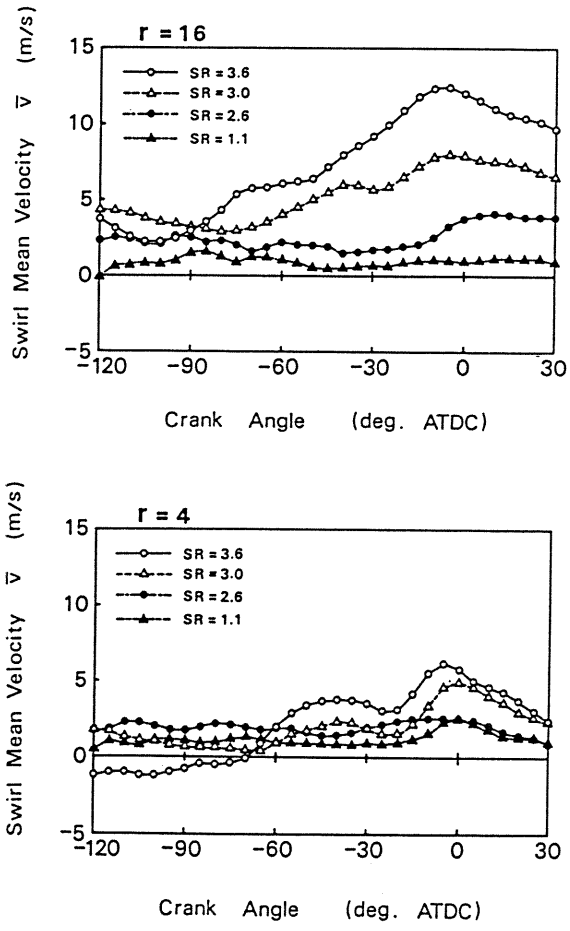

Fig.12 Velocity variations versus crank-angle for different swirl ratios at r = 16 and r = 4 (bowl piston, 600 rpm)

following definition.

$$SRe = \frac{30}{\pi Ne} \cdot \frac{4\int_0^{r_{max}} r^2 \cdot \bar{v}(r)\, dr}{r_{max}^4} \qquad (2)$$

where, r is radial distance, $\bar{v}$ is swirl mean velocity, and Ne is engine speed. In equation (2), the range of integration corresponds to the measurement range of radial direction.

The results are plotted against the steady-state swirl ratio of intake port in Figure 13. As seen in the figure, a considerable difference between the cases of flat piston and bowl piston appears in the relation of the equivalent ratio to the steady-state swirl ratio. In the case of flat piston, the linear relationship between the two kinds of ratios is apparent. And the equivalent ratio at TDC is approximately comparable with the steady-state ratio in quantity. In this case, the swirl velocity profile has almost the solid body rotation pattern, as mentioned previously. Therefore, this result suggests that the swirl velocity at TDC is roughly predictable from the steady-state swirl ratio. On the other hand, in the case of bowl piston, the relation between the two kinds of ratios indicates non-linearity, and presents an inflection point in the curve at the steady-state ratio of 2.6-3.0. As the steady-state ratio becomes higher than that of the point, the equivalent ratio at TDC remarkably increases, compared with those of flat piston. But at lower steady-state ratios, the increase of equivalent ratio at TDC is not so large as that at higher steady-state ratios, which is attributed to the fact that the velocity profile becomes considerably non-linear. This result indicates that in the case of bowl piston the flow field near TDC cannot be predicted by the swirl ratio alone.

CONCLUSION

The swirl flow has been investigated under

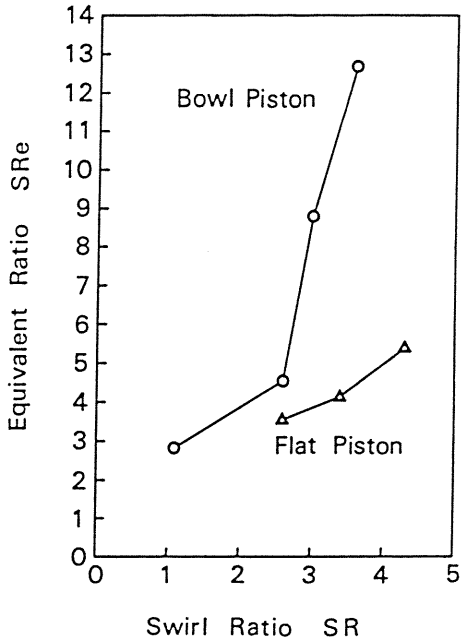

Fig.13 Relations between the steady-state ratio of intake port (SR) and that determined from the measured velocity at TDC (SRe) for different chamber cases

motored condition by use of a newly-developed experimental system, comprising a backscatter LDV and a "bottom-view engine" with the same intake port configuration and valve locations as those of actual engines.

The experimental results may be summarized as follows.

(1) The relation between the in-cylinder swirl characteristics and the steady-state swirl ratio of intake port is different from the case of flat piston and the case of bowl piston. The swirl velocity profile against the ratio has the following implications for either case.

(a) In the case of flat piston, the swirl mean velocity profiles during compression and early expansion stroke have almost the solid body rotation configurations irrespective of the swirl ratio of the intake port.

(b) In the case of cylindrical bowl piston, the swirl mean velocity profiles near TDC are no longer similar for different swirl ratios. At higher ratios, the profile remains nearly linear, but, at lower ratios, it becomes non-linear.

(2) The equivalent ratio determined from the measured swirl velocity profile at TDC depends upon the steady-state swirl ratio of intake port. But their changing manners against the steady-state ratio are also different for two chamber cases as follows.

(a) The flat piston case shows an approximate linear relation between the two ratios. The equivalent ratio is approximately comparable with the steady-state swirl ratio in quantity.

(b) The bowl piston case has non-linear relation and shows the presence of an inflection point in the curve. The equivalent ratio largely increases as steady-state ratio increases, but does not so much increase at lower ratios which reflects the non-linear velocity profile.

REFERENCES

1. Fitzgoerge, D., and Allison, J. L., "Air Swirl in a Road-Vehicle Diesel Engine," Proc. Instn. Mech. Engrs. (A.D.), No.4, 1962-1963.
2. Uzkan, T., Borgnakke, C., and Morel, T., "Characterization of Flow Produced by a High-Swirl Inlet Port," SAE Paper No.830266, 1983.
3. Dyer, T. M., "New Experimental Techniques for In-Cylinder Engine Studies," SAE Paper No.850396, 1985.
4. Asanuma, T., and Obokata, T., "Gas Velocity Measurements of a Motored and Firing Engine by Laser Anemometry," SAE Paper No.790096, 1976.
5. Rask, R. B., "Laser Doppler Anemometer Measurement in an Internal Combustion Engine," SAE Paper No.790094, 1979.
6. Wigley, G. and Renshaw, J., "In-Cylinder Swirl Measurement by Laser Anemometry in a Production Diesel Engine," Report AERE-R9651, AERE Harwell, 1979.
7. Jonston, S. C., Robinson, C. W., Rorke, W. S., Smith, J. R., and Witze, P. O., "Applicaion of Laser Diagnostics to an Injected Engine," SAE Paper No.790092, 1979.
8. Arcoumanis, C., Bicen, A. F., and Whitelaw, J. H., "Squish and Swirl-Squish Interaction in Motored Model Engines," J. Fluids Engineering, Vol. 105, pp. 105-112, 1983.
9. Witze, P. O., Martin, J. K. and Borgnakke, C., "Measurementa and Predictions of the Precombustion Fluid Motion and Combustion Rates in a Spark Ignition Engine," SAE Paper No.831697, 1983.
10. Wigley, G., Patterson, A. C., and Renshaw, J., "The Use of Laser Anemometry to Measure Swirl Velocity in a Firing Production Diesel Engine," Report AERE-R10692, AERE Harwell, 1982.
11. Ball, W. F., Pettifer, H. F., and Woterhouse, C. N. F., "Laser Doppler Velocimeter Measurements of Turbulence in a Direct-Injection Diesel Combustion Chamber," Proc. I. Mech. E. Conf. on combustion in Engineering, Vol. 1, Paper No. C52/83, pp. 163-174, 1983.
12. Liou, T. -M., Hall, M., Santavicca, D. A., and Bracco, F. V., "Laser Doppler Velocimetry Measurements in Valved and Ported Engines," SAE Paper No.840375, 1984.
13. Matsuoka, S., Kamimoto, T., Urushihara, T., Mochimaru, Y., and Morita, H., "LDA Measurement and a Theoretical Analysis of the In-cylinder Air Motion in a DI Diesel Engine," SAE Paper No.850106, 1985.
14. Fansler, T. D., "Laser Velocimetry Measurements of Swirl and Squish Flows in an Engine with a Cylindrical piston Bowl," SAE Paper No.850124, 1985.
15. Brandstätter, W., Johns, R. J. R., and Wigley, G., "The Effect of Inlet Port Geometry in In-Cylinder Flow Structure," SAE Paper No.850499, 1985.
16. Kondoh, T., Fukumoto, A., Ohsawa, K., Ohkubo, Y., "An Assessment of Multi-Dimensional Numerical Method to Predict the Flow in Internal Combustion Engines," SAE Paper No.850500, 1985.